

Wavelet Coherence Model for Diagnosis of Alzheimer Disease

Clinical EEG and Neuroscience
00(0) 1-11
© EEG and Clinical Neuroscience
Society (ECNS) 2012
Reprints and permission:
sagepub.com/journalsPermissions.nav
DOI: 10.1177/1550059412444970
http://eeg.sagepub.com



Ziad Sankari¹, Hojjat Adeli², and Anahita Adeli³

Abstract

This article presents a wavelet coherence investigation of electroencephalograph (EEG) readings acquired from patients with Alzheimer disease (AD) and healthy controls. Pairwise electrode wavelet coherence is calculated over each frequency band (delta, theta, alpha, and beta). For comparing the synchronization fraction of 2 EEG signals, a wavelet coherence fraction is proposed which is defined as the fraction of the signal time during which the wavelet coherence value is above a certain threshold. One-way analysis of variance test shows a set of statistically significant differences in wavelet coherence between AD and controls. The wavelet coherence method is effective for studying cortical connectivity at a high temporal resolution. Compared with other conventional AD coherence studies, this study takes into account the time–frequency changes in coherence of EEG signals and thus provides more correlational details. A set of statistically significant differences was found in the wavelet coherence among AD and controls. In particular, temporocentral regions show a significant decrease in wavelet coherence in AD in the delta band, and the parietal and central regions show significant declines in cortical connectivity with most of their neighbors in the theta and alpha bands. This research shows that wavelet coherence can be used as a powerful tool to differentiate between healthy elderly individuals and probable AD patients.

Keywords

Alzheimer disease, electroencephalography, wavelet coherence, functional connectivity, wavelet coherence fraction

Received November 6, 2011; accepted January 27, 2012.

Introduction

Alzheimer disease (AD) is characterized by 2 histological features: amyloid plaques and neurofibrillary tangles. In addition, it is characterized by a loss of functional connections between different areas of the brain.¹ While modern imaging techniques are unable to detect the histological features of AD, electroencephalography (EEG) remains a powerful tool providing high temporal and spatial resolution to study functional connections within different areas of the brain.²⁻¹² Electroencephalogram signals are commonly decomposed into subbands: delta (0-4 Hz), theta (4-8 Hz), alpha (8 to 12 Hz), and beta (12 to 30 Hz). Each of the subbands relates to different functional and physiological parts of the brain. Adeli et al¹³ present a spatio-temporal wavelet chaos methodology for the analysis of EEGs and their delta, theta, alpha, and beta subbands for discovering potential markers of abnormality in AD.

Coherence is one way to study cortical connectivity in the human brain. Recently, Sankari, Adeli, and Adeli¹⁴ presented an EEG coherence study of AD and found statistically significant differences in electrode coherence between AD and controls. While conventional coherence remains a common tool to study cortical connectivity, its drawback is that only spectral components are observed while temporal data are completely lost. Hence, time–frequency analysis methods can be used to study the changes in cortical connectivity over time. One way

to achieve this is by using the short-time Fourier transform (STFT) where a fixed sliding window provides EEG spectral analysis within the time covered by this window. Although it presents spectral and temporal information, STFT has drawbacks such as a fixed sliding window size which is not optimal for different signal frequencies. As such, STFT is not the most suitable approach for EEG studies. A more recent concept used over the past two decades is wavelet analysis.¹⁵⁻¹⁷

In wavelet analysis, a base window function, called a mother wavelet, is scaled and translated to be used in the analysis of a time signal.¹⁸⁻²¹ Wavelet analysis of EEG signals has been employed by a number of researchers^{13,22-24} for feature extraction

¹ Departments of Biomedical Engineering, Electrical and Computer Engineering, Ohio State University, OH, USA

² Departments of Biomedical Engineering, Biomedical Informatics, Civil and Environmental Engineering and Geodetic Science, Electrical and Computer Engineering, Neurological Surgery, and Neuroscience, Ohio State University, Columbus, OH, USA

³ Department of Neurology, Mayo Clinic, Rochester, MN, USA

Corresponding Author:

Hojjat Adeli, Departments of Biomedical Engineering, Biomedical Informatics, Civil and Environmental Engineering and Geodetic Science, Electrical and Computer Engineering, Neurological Surgery, and Neuroscience, Ohio State University, 470 Hitchcock Hall, 2070 Neil Avenue, Columbus, OH 43210, USA
Email: adeli.1@osu.edu

or denoising of EEG signals. Torrence and Campo²⁵ proposed a wavelet coherence (WC) method for the analysis of spectral and temporal synchronization²⁶ between 2 signals for geophysical applications in order to incorporate the temporal aspect into their analysis. Subsequently, other researchers used WC in geophysical applications.^{27,28} Lachaux et al²² provided the proof of concept for application of WC in EEG analysis. They applied it only to a single sample EEG, with no association with any disorder. Klein et al²⁹ compare conventional and WC using EEG data of 26 participants obtained in an experiment on associative learning. They conclude that WC can detect features of synchrony undetectable by conventional coherence. Sakkalis et al³⁰ applied a WC model to EEGs from patients with schizophrenia to study the “disconnection syndrome” in the brain. The results are consistent with previous neural connection disturbance findings. The study provides additional information related to the location of most prominent disconnections.

Adeli et al³¹ present a review of research performed on computational modeling of AD and its markers with a focus on computer imaging, classification models, connectionist neural models, and biophysical neural models. Adeli et al³² present a review of models of computation and analysis of EEGs for diagnosis and detection of AD. Their review covers 3 areas: time-frequency analysis, wavelet analysis, and chaos analysis.

In this article, a WC investigation of EEG readings acquired from AD patients and healthy controls is presented. To the best of the authors’ knowledge, this is the first time WC is applied to AD data in an attempt to distinguish between AD and controls.

Data Acquisition

The EEGs were obtained from 20 patients (average age of 74) diagnosed with probable AD per National Institute of Neurological and Communicative Disorders and Stroke (NINCDS); Alzheimer’s Disease and Related Disorders Association (ADRDA) and *Diagnostic and Statistical Manual of Mental Disorder* (Third Edition Revised; *DSM-III-R*) criteria and 7 healthy (control) participants (average age of 71), using a standard 10-20 electrode configuration on the scalp.³³ Recordings from 19 scalp electrodes: Fp2, Fp1, F7, F3, Fz, F4, F8, T3, C3, Cz, C4, T4, T5, P3, Pz, P4, T6, O2, and O1 (Figure 1) are taken while the participants’ eyes are closed. Temporal behavior is examined by accumulating data at a sampling rate of 128 Hz for epochs of 8 seconds, resulting in time series of 1024 data points. Digital conversion of the measured analog signal is accomplished with an 8-bit digitizer. A band-pass filter (0.1-30 Hz, -12 dB/octave roll-off) is used to filter the frequency band of interest. The EEGs are visually inspected and discriminated to eliminate those time series that contain optical and muscular artifacts.

Methods

Conventional Coherence

Conventional coherence for 2 signals x and y is defined as the magnitude square of the cross-spectrum of the signals divided

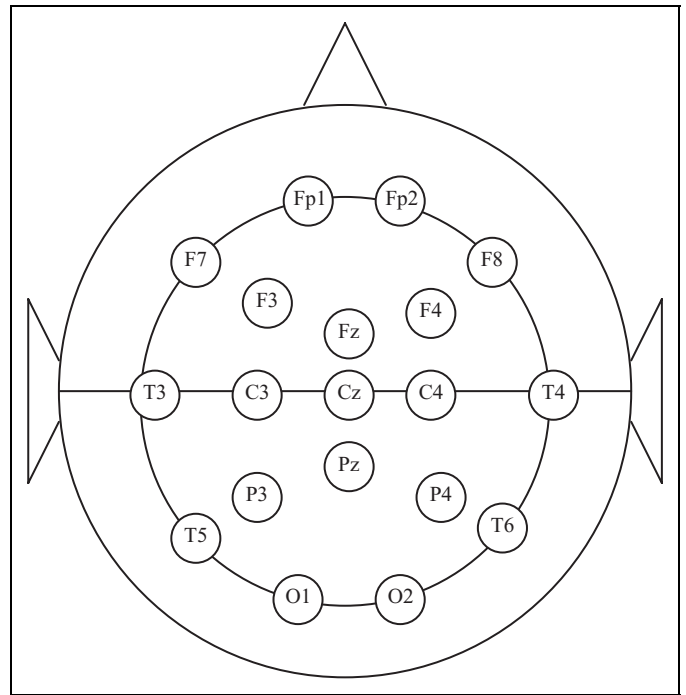


Figure 1. Nineteen electroencephalogram (EEG) electrodes in the International 10-20 System.

by the product of the power spectral densities (PSDs) of each of the signals:

$$C_{xy}(f) = \frac{|W_{xy}|^2(f)}{W_x(f)W_y(f)} \quad (1)$$

where f is the frequency, W_x is the PSD of x , W_y is the PSD of y , and W_{xy} is the cross-spectral density of the 2 signals x and y . The cross-power spectrum in equation (1) is defined as:

$$W_{xy}(f) = X(f)Y^*(f) \quad (2)$$

where $X(f)$ is the fast Fourier transform (FFT) of x and $Y(f)$ is the FFT of y . Throughout this article, the asterisk sign $*$ is used to denote the complex conjugate operator. Equation (2) requires x and y to have infinite time support. In practice, signals have limited time support and equation (2) is typically estimated using a temporal smoothing operation, such as the weighted overlapping segment averaging (WOSA).²² The WOSA divides each time signal into N overlapping partitions, each weighted by a windowing function (Hann, Hamming, etc). The FFT is applied to each of the N segments and an averaging process is used to estimate the PSDs and the cross-spectral density.

Wavelet Coherence

The definition of coherence presented above is suitable for time signals with fixed spectral characteristics. Such signals, called stationary, have a nonvarying FFT spectrum over time.²² The EEG signals, however, are recordings of brain activities and are far from being stationary as their spectral characteristics vary widely over time.^{29,34,35} Thus, a time-varying spectral

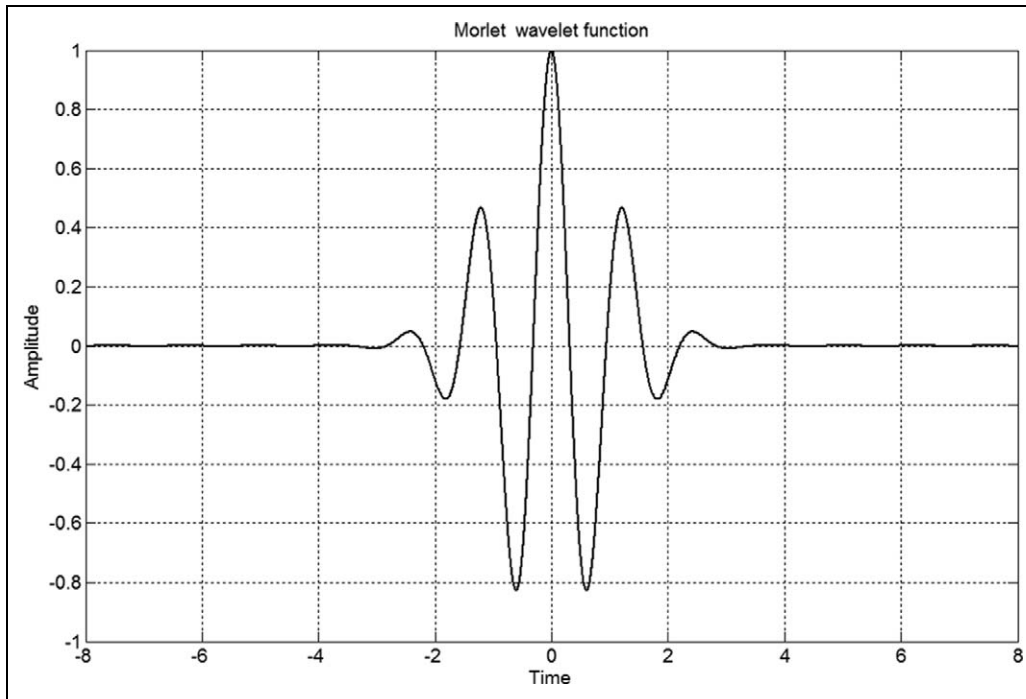


Figure 2. Morlet wavelet.

Table 1. Adjacency List

Electrode	Adj1	Adj2	Adj3	Adj4	Adj5	Adj6	Adj7	Adj8
1	Fp1	Fp2	F7	F3	Fz			
2	Fp2	Fp1	Fz	F4	F8			
3	F7	Fp1	F3	T3	C3			
4	F3	Fp1	F7	Fz	T3	C3	Cz	
5	Fz	Fp1	Fp2	F3	F4	C3	Cz	C4
6	F4	Fp2	Fz	F8	Cz	C4	T4	
7	F8	Fp2	F4	C4	T4			
8	T3	F7	F3	C3	T5	P3		
9	C3	F7	F3	Fz	T3	Cz	T5	P3
10	Cz	F3	Fz	F4	C3	C4	P3	Pz
11	C4	Fz	F4	F8	Cz	T4	Pz	P4
12	T4	F4	F8	C4	P4	T6		
13	T5	T3	C3	P3	O1			
14	P3	T3	C3	Cz	T5	Pz	O1	
15	Pz	C3	Cz	C4	P3	P4	O1	O2
16	P4	Cz	C4	T4	Pz	T6	O2	
17	T6	C4	T4	P4	O2			
18	O1	T5	P3	Pz	O2			
19	O2	Pz	P4	T6	O1			

coherence is necessary to investigate the changes in cortical connectivity. In this research continuous wavelet transform (CWT) is used for time–frequency analysis. The CWT of a time signal x is defined as³⁶:

$$CWT_x(\tau, a) = \int_{-\infty}^{+\infty} x(t)\Psi_{\tau,a}(t)dt \quad (3)$$

where t is time and $\Psi_{\tau,a}(t)$ is a version of the base function known as mother wavelet that is scaled by a and shifted by τ .

Table 2. Electrode Pairs in the Delta Band Showing Statistically Significant Differences in the Wavelet Coherence Fraction (CF) Among Alzheimer disease (AD) Group and Healthy Controls ($P < .01$)

Electrode	Adjacent Electrode	Healthy CF	AD CF
T3	C3	0.5497	0.1333
	T5	0.423	0.0784
C3	T5	0.5504	0.1053
C4	T6	0.6422	0.216
T5	C3	0.5504	0.1053
	P3	0.5502	0.1764
T6	O2	0.6256	0.1695

As such, the CWT of a time signal is a function of time and scale a . The scale is related to the central frequency of a shifted and scaled wavelet. Therefore, when performing CWT analysis using a particular wavelet, each scale corresponds to a specific frequency. The reader should refer to Daubechies,³⁶ Mallat,³⁷ and Adeli and Ghosh-Dastidar³⁸ for details of wavelet transforms.

There is a variety of wavelet functions that differ in shape and properties. The choice of a wavelet depends on the application.^{39–45} For EEG analysis using WC^{22,29} as well as other applications of WC,²⁸ Morlet wavelet has been proved as a good choice because it has a simple and smooth spectrum and represents a good balance between time and frequency localization. Morlet wavelet is defined as (Figure 2):

$$\Psi_0(t) = \pi^{-0.25} e^{i2\pi ft} e^{-0.5t^2} \quad (4)$$

The CWT in equation (3) is computed by filtering the time signal x through time-shifted and scaled versions of equation (4).

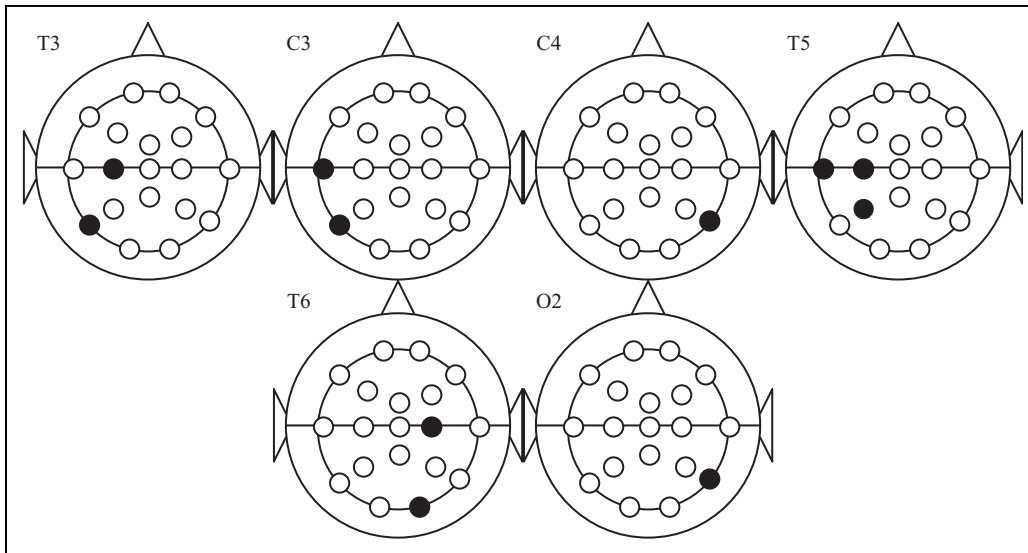


Figure 3. Electrode pairs in the delta band showing statistically significant differences in the wavelet coherence fraction (CF) among Alzheimer disease (AD) group and controls ($P < .01$).

Table 3. Electrode Pairs in the Theta Band Showing Statistically Significant Differences in the Wavelet Coherence Fraction (CF) Among Alzheimer disease (AD) Group and Healthy Controls ($P < .01$)

Electrode	Adjacent Electrode	Healthy CF	AD CF
F3	C3	0.6168	0.3674
	Cz	0.5709	0.2826
Fz	C3	0.6239	0.3252
	Cz	0.6039	0.2866
F4	Cz	0.609	0.2721
	C4	0.5824	0.3556
T3	T4	0.5516	0.3135
	C3	0.5876	0.312
C3	T5	0.57	0.1861
	P3	0.5884	0.1994
	Cz	0.66	0.2752
Cz	T5	0.5459	0.2053
	P3	0.6087	0.2542
	Pz	0.6013	0.1505
	C4	0.6353	0.3838
C4	P3	0.5831	0.2555
	Pz	0.5919	0.2548
	P4	0.6074	0.2922
	Pz	0.5834	0.1763
T4	P4	0.6	0.2402
	T6	0.5751	0.2123
	P4	0.5741	0.2875
T5	T6	0.5827	0.3071
	P3	0.6164	0.2894
P3	O1	0.6071	0.257
	Pz	0.6567	0.2896
	O1	0.6279	0.1848
Pz	P4	0.6204	0.2651
	O1	0.5844	0.2425
	O2	0.635	0.1898
P4	O2	0.6147	0.1234

The wavelet power (WP) of a signal x is defined as the norm square of the CWT of x :

$$WP_x(t, f) = \|CWT_x(t, f)\|^2 \quad (5)$$

and is a function of time t and wavelet center frequency f . (The center frequency of a wavelet function is the center of the FFT spectrum of that particular wavelet function.)

The cross-wavelet transform (XWT) between 2 signals x and y , a measure of signal areas with high common power, is defined as:

$$XWT_{xy}(t, f) = CWT_x(t, f) \cdot CWT_y^*(t, f) \quad (6)$$

Similar to conventional coherence and following Torrence and Webster,²⁷ Lachaux et al,²² and Grinsted et al,²⁸ a smoothing operation is used to estimate WC. The smoothing operation depends on the wavelet type and scales used as illustrated shortly. Smoothing takes place across scale and time axes; it increases the degree of freedom for each point in the CWT.²⁵ A proper smoothing function for WC application across time axis S_{time} is defined for the Morlet wavelet as²⁸:

$$S_{time}(CWT_x(t, f)) = CWT_x(t, f) \wedge c_1^{-\frac{\lambda^2}{2}} \quad (7)$$

where $\lambda = t/a$, c_1 is a normalization constant, and \wedge refers to the convolution operator. The smoothing function across scale S_{scale} (frequency) axis is defined as²⁸:

$$S_{scale}(CWT_x(t, f)) = CWT_x(t, f) \wedge c_2 \Pi(0.6a) \quad (8)$$

where c_2 is a normalization constant, and Π is the rectangular function. In practice, the 2 convolutions in equations (7) and (8) are computed discretely and the normalization coefficients are determined numerically. The width of the rectangular function Π used in S_{scale} is determined by the scale-decorrelation length that is empirically determined to be 0.6 for the Morlet wavelet.²⁵

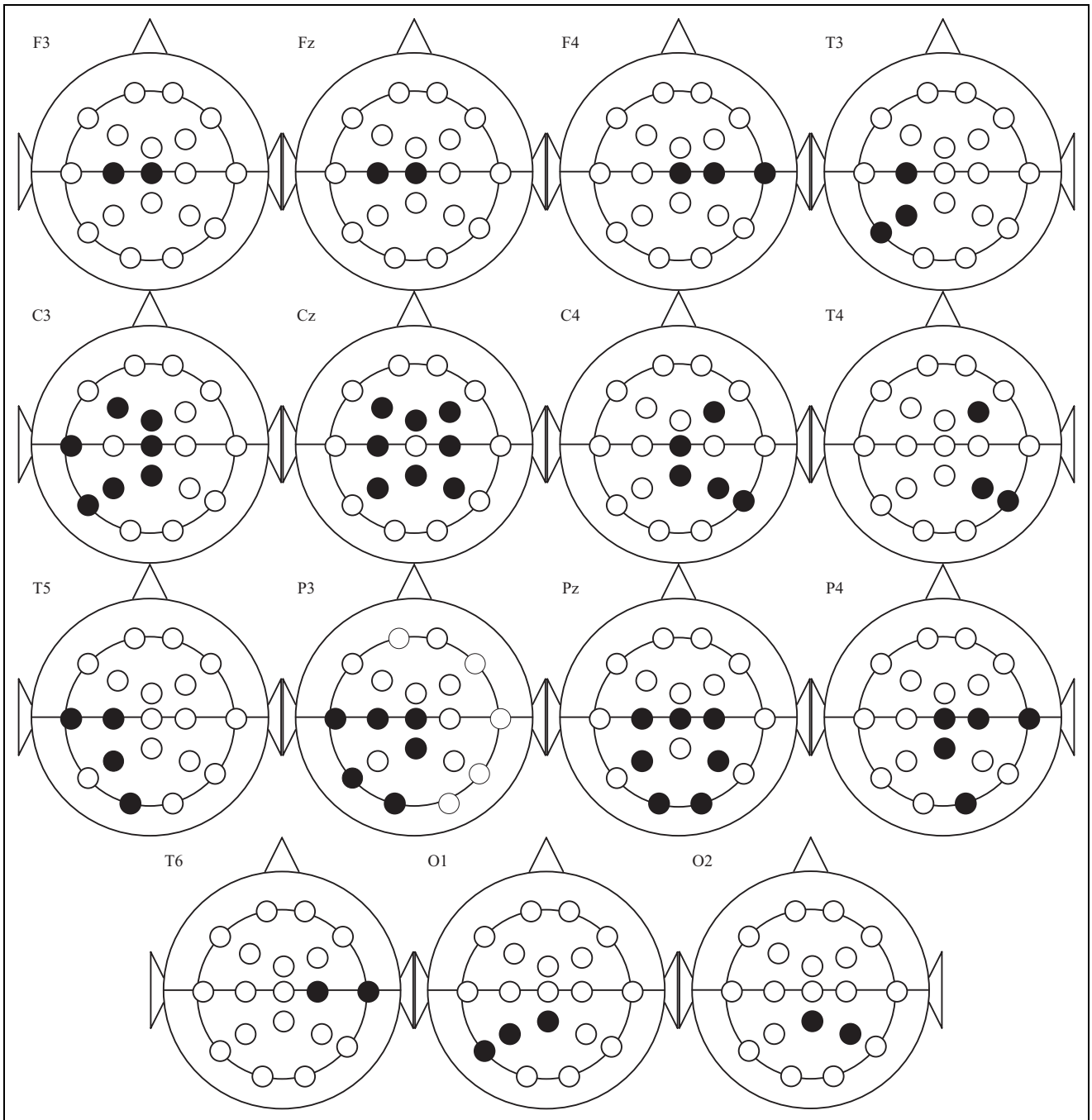


Figure 4. Electrode pairs in the theta band showing statistically significant differences in the wavelet coherence fraction (CF) among Alzheimer disease (AD) group and controls ($P < .01$).

Having defined the smoothing functions, the WC is defined as:²⁸

$$WC_{xy}(t,f) = \frac{|S(a^{-1}XWT_{xy}(t,f))|^2}{S(a^{-1}WP_x(t,f))S(a^{-1}WP_y(t,f))} \quad (9)$$

where the scale inverse a^{-1} is used to normalize the XWT.²⁷ The Schwartz inequality ensures that WC_{xy} has values between 0 and 1.²² The smoothing operator S is applied such that²⁸:

$$S(w) = S_{scale}[S_{time}(W)] \quad (10)$$

Adjacency List and EEG Subbands

The EEG recordings in this research are taken from 19 electrodes in the 10-20 International System (Figure 1). Since the instantaneous coherence is being investigated via wavelet analysis, only adjacent (local) electrode pairs are studied to avoid faulty results due to propagation delays and other electrical effects observed within a volume conduction scheme when distal electrodes are considered. Local pairs of electrodes are defined as electrodes immediately adjacent

Table 4. Electrode Pairs in the Alpha Band Showing Statistically Significant Differences in the Wavelet Coherence Fraction (CF) Among Alzheimer disease (AD) and Healthy Controls ($P < .01$)

Electrode	Adjacent Electrode	Healthy CF	AD CF
F3	C3	0.648	0.3322
	Cz	0.6067	0.3104
Fz	C3	0.6066	0.323
	Cz	0.6408	0.3212
F4	C4	0.6179	0.3892
	Cz	0.6304	0.3159
	C4	0.6412	0.4008
	T4	0.5663	0.3258
C3	Cz	0.6324	0.3541
	P3	0.6182	0.3772
Cz	Pz	0.6074	0.2729
	C4	0.6564	0.3878
	P3	0.6002	0.3725
	Pz	0.6246	0.3158
C4	P4	0.606	0.3343
	Pz	0.612	0.3725
	P4	0.6187	0.3158
	T6	0.5678	0.3343
T4	P4	0.5725	0.3275
P3	Pz	0.6509	0.4425
	O1	0.6459	0.3152
Pz	P4	0.665	0.3493
	O2	0.6147	0.3326
P4	O2	0.6399	0.2879
O1	O2	0.6383	0.34

on the scalp. Each electrode has 4 to 8 adjacent electrodes organized in an adjacency list (Table 1).

In this research, WC is investigated within each of the 4 aforementioned subbands separately. The WC fluctuates in different bands and the fluctuation in the full band-limited EEG is so large that it does not yield any useful information.

Adjacency lists for the 19 scalp electrodes are constructed (Table 1) and a wavelet coherence fraction ([CF] detailed below) is calculated for each adjacent electrode pairs.

Wavelet Coherence Fraction

In this research, an average WC is computed over each of the 4 aforementioned bands by averaging the WC coefficients in $WC_{xy}(t, f)$ as follows:

$$A_{xy}(t) = \frac{1}{U-L} \int_L^U WC_{xy}(t, f) df \quad (11)$$

where A_{xy} is the frequency averaged WC function in each band, and U and L are the upper and lower frequency bounds of the band, respectively. From this point onward, this function is referred to simply as WC.

In order to interpret the results of WC, it is necessary to devise a scheme to compare the results of AD and control

groups quantitatively and qualitatively. In this research, the authors propose wavelet coherence fraction (CF) for comparing the synchronization fraction of 2 EEG signals. It is defined as the fraction of the signal time during which the WC value is above a certain threshold. As such, CF varies between 0 and 1. The reference threshold is chosen to be the average of $A_{xy}(t)$ values for all healthy/control EEGs over time. As such for electrode pairs x and y , the threshold T_B in band B is computed as follows:

$$T_B = \frac{\sum_1^{N_h} \text{mean}[A_{xy}(t)]}{N_h} \quad (12)$$

where N_h is the number of control EEGs, $\text{mean}[A_{xy}]$ is the group mean of the frequency averaged WC functions for electrodes x and y of control participants.

Analysis of variance (ANOVA) is applied to find statistically significant differences between AD and control groups using $P < .01$.

Results

Table 2 and Figure 3 present electrode pairs with statistically significant ($P < .01$) differences in the delta band, and the group average CF for AD group and controls. In this band, the AD group shows a statistically significant ($P < .01$) decrease in CF compared with the healthy controls in the left temporocentral and temporoparietal areas, and in the right temporocentral and temporooccipital areas. In general, the delta band exhibits the lowest CF values for the AD group compared with all other frequency bands.

Table 3 and Figure 4 show electrode pairs with statistically significant ($P < .01$) differences in the theta band and the group average CF for AD group and controls. In this band, a decrease in CF is observed in most local electrode pairs. The AD group shows decreased values of CF with statistical significance in both left and right hemispheres. The only electrode pairs that do not show statistically significant changes in CF values are frontopolar (Fp1 and Fp2) and frontal electrodes (F7 and F8). The central and frontal electrodes along the midline of the scalp (Cz and Fz) in particular show significant decrease in CF with all neighboring electrodes.

Table 4 and Figure 5 show electrode pairs with statistically significant ($P < .01$) differences in the alpha band and the group average CF for AD group and controls. In the alpha band, a pattern of significant decrease in CF similar to the theta band is observed in patients with AD. Most electrode pairs show a statistically significant decrease in CF values with their neighboring electrodes. The exceptions are frontopolar electrodes (Fp1 and Fp2), frontal electrodes (F7 and F8), and left temporal electrodes (T3 and T5) which do not show a significant change in CF values when compared with controls. Similar to what is observed in the theta band, the central midline electrode (Cz) shows a significant decrease with all its neighbors. A finding exclusive to this band is that the midline parietal electrode (Pz) shows a significant decrease with all neighbors except the left occipital electrode (O1). In general, the alpha band exhibits

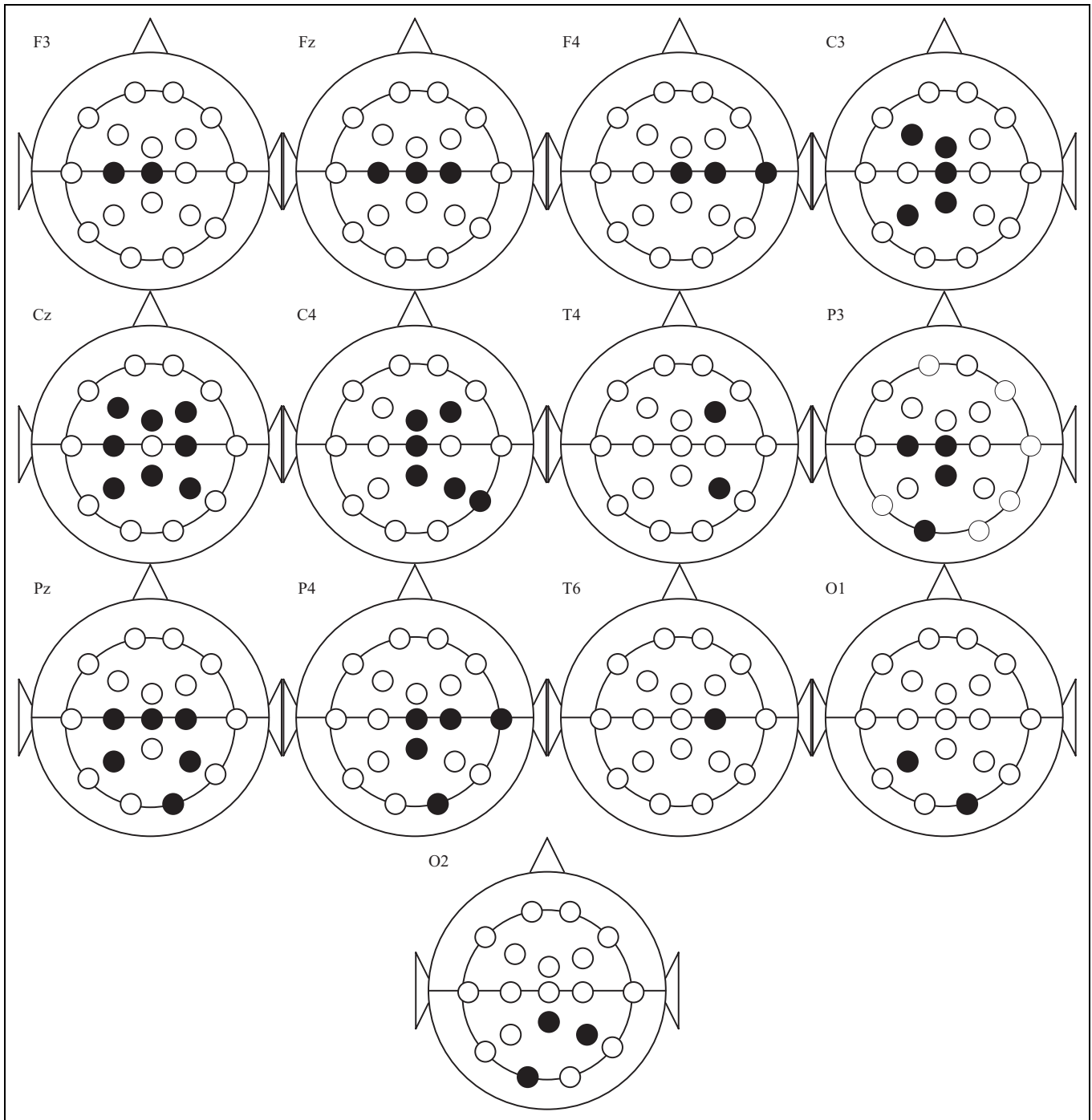


Figure 5. Electrode pairs in the alpha band showing statistically significant differences in the wavelet coherence fraction (CF) among Alzheimer disease (AD) and controls ($P < .01$).

the highest CF values for both AD and control groups compared with other frequency bands.

Table 5 and Figure 6 show electrode pairs with statistically significant ($P < .01$) differences in the beta band and the group average CF for AD and controls. In this band, the CF values for controls are generally the lowest compared with other bands, while the CF values for AD are not the lowest. In the beta band,

most electrode pairs show significant decrease in AD CF values compared with the control group. Exceptions that do not present a significant change in CF values include frontopolar electrodes (Fp1 and Fp2), right frontal electrode (F8), and right temporal electrode (T4). The parietal midline electrode shows a significant decrease in CF values with all its neighbors except (P3). The occipital electrodes (O1 and O2) show significant

Table 5. Electrode Pairs in the Beta Band Showing Statistically Significant Differences in the Wavelet Coherence Fraction (CF) Among Alzheimer disease (AD) and Healthy Controls ($P < .01$)

Electrode	Adjacent Electrode	Healthy CF	AD CF
F7	T3	0.5096	0.2794
	C3	0.5176	0.2493
F3	T3	0.4826	0.2954
	C3	0.5753	0.3112
Fz	Cz	0.5861	0.2427
	C3	0.5578	0.3284
F4	Cz	0.648	0.2832
	Cz	0.5756	0.2778
T3	T5	0.5347	0.2655
C3	Pz	0.5465	0.2885
Cz	C4	0.5875	0.3704
	Pz	0.5887	0.3372
C4	Pz	0.5558	0.2967
	P4	0.5883	0.3307
T5	T6	0.5131	0.2612
	P3	0.5731	0.3841
P3	O1	0.5921	0.2889
	O1	0.6046	0.2441
Pz	P4	0.6035	0.3341
	O1	0.5763	0.2878
P4	O2	0.5664	0.2523
	T6	0.5745	0.3177
T6	O2	0.5917	0.1831
	O2	0.5954	0.266
O1	O2	0.5897	0.2809

decrease in CF values with all their neighbors, a finding that is unique to the beta band.

In general, the CF values for AD participants are lower than in controls. Higher values are observed in the delta band in the frontal–frontopolar electrode pairs, and in the theta and alpha bands in the frontopolar pairs. However, these values do not reach statistical significance. The observed decrease in CF values for AD is manifested differently among neighboring electrodes within each band.

Discussion

In this research, a wavelet CF is introduced and investigated as a measure of pairwise EEG electrode synchronization and, hence, cortical connectivity. In order to compare the AD and control participants, the CF value is calculated with reference to a threshold value (T_B) that depends on the average coherence values of control participants. As an example, a CF value of 0.6 for a particular electrode pair indicates that the instantaneous WC of this pair is 60% of the time above the threshold T_B (determined by healthy controls). The WC method is effective for studying cortical connectivity at a high temporal resolution. Compared with other conventional AD coherence studies,⁴⁶⁻⁴⁹ this study takes into account the time–frequency changes in coherence of EEG signals and thus provides more correlational details.

Using conventional coherence to study the EEG of patients with AD, Besthorn et al⁴⁶ find no significant differences between AD group and controls in the delta band. On

the other hand, this study shows a significant decrease in AD CF values in a set of electrode pairs within the delta band in the left temporocentral, temporoparietal, and the right temporocentral and temporooccipital areas of the brain.

Bablioni et al⁴⁸ report a decreased frontoparietal coherence (F3-F4 and P3-P4) in AD patients over the alpha, beta1 (14-16 Hz), and beta2 (20-22 Hz) bands. Jelles et al⁴⁹ use global conventional coherence as a measure of EEG coherence in AD group. They find no significant global coherence differences in the delta, theta, and alpha1 (7-10 Hz) bands, but report a decrease in AD global coherence in the alpha2 (10-13 Hz) and beta bands. In contrast to these 2 studies, this research finds a statistically significant decrease in WC in all bands, with a specific pattern within each band. Conventional coherence studies reflect only a single dimension of coherence, that is, frequency.

Recently, Sankari, Adeli, and Adeli^{14,50} found a set of statistically significant changes in AD coherence compared with controls. They reported that electrode F3 shows the least pairwise significance in all bands, indicating that electrode F3 is perhaps not useful for collecting information for diagnosis of AD. In contrast, this study shows that the WC between F3 and neighboring electrodes exhibits a statistically significant decrease in the theta, alpha, and beta bands. This leads to the conclusion that the WC method is more powerful in detecting differences in coherence among AD and control groups than the conventional coherence. The current WC study detects significant differences between AD participants and controls

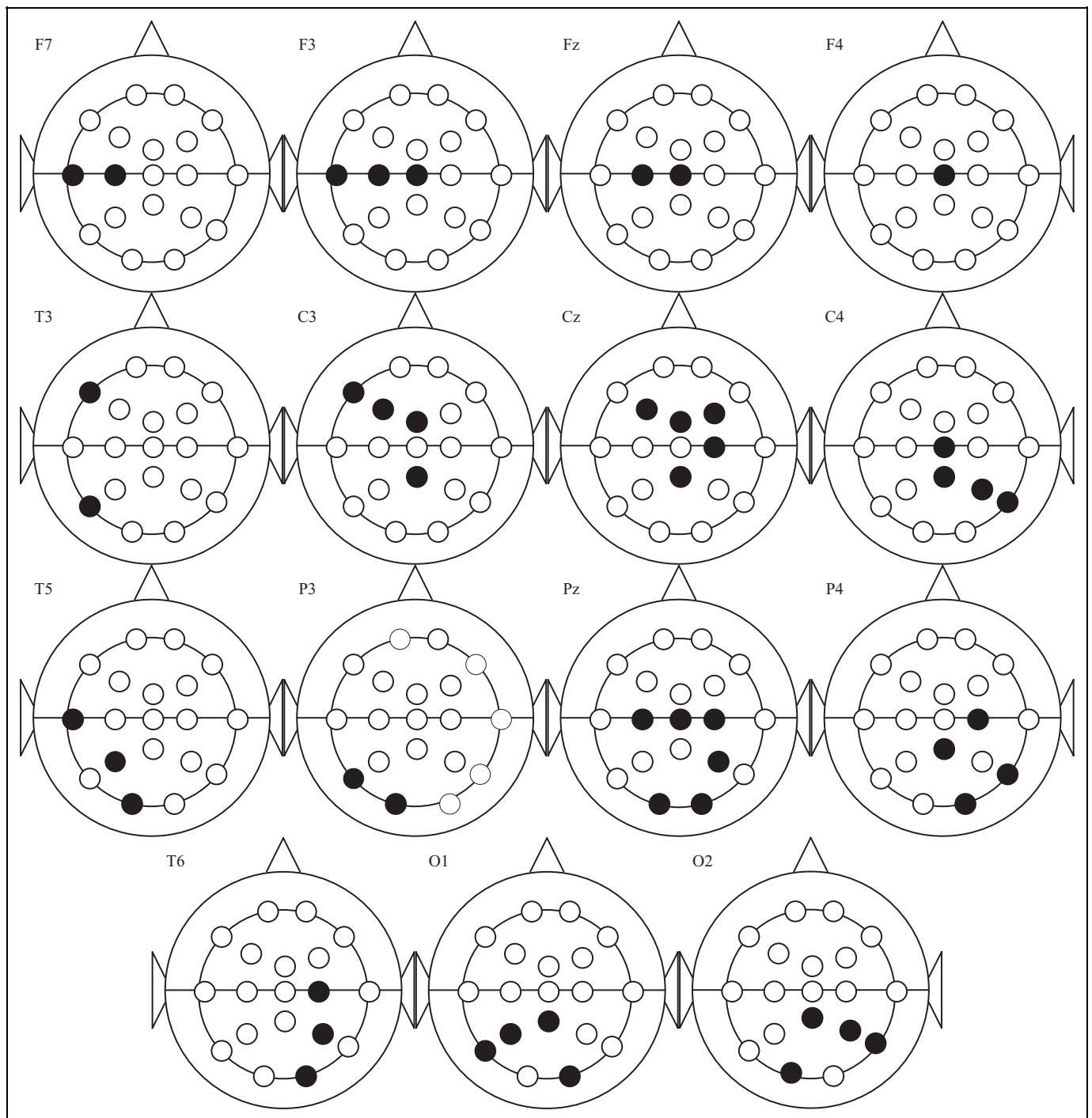


Figure 6. Electrode pairs in the beta band showing statistically significant differences in the wavelet coherence fraction (CF) among Alzheimer disease (AD) and controls ($P < .01$).

in pairs of electrodes such as C3 and Cz in the theta band, and O1 in the beta band, not observed in the previous conventional coherence study reported by the authors.

When compared with the condition of healthy elderly individuals (controls), the decrease in WC observed in AD group is attributed to a loss in cortical connectivity in the AD brain. In general, this loss of connectivity in AD can, in turn, be attributed to a loss of axonal connections among

different areas of the brain as amyloid plaques and neurofibrillary tangles form. This formation hinders the smooth electric communication between different parts of the brain.

Conclusion

Compared with conventional coherence, WC is a more detailed way to study cortical connectivity in patients with AD because

it incorporates both temporal and spectral information. A set of statistically significant differences was found in the WC among AD group and controls. In particular, the temporocentral regions show significant decrease in WC in AD in the delta band, and the parietal and central regions show significant declines in cortical connectivity with most of their neighbors in the theta and alpha bands. This study further shows that the beta bands of occipital EEGs are significant for diagnosis of AD, a finding not noted in the previous research using conventional coherence. To sum it up, studies of WC in local electrodes provide deeper insights about cortical connectivity in the brain of AD participants compared to conventional coherence methods. This article lays the foundation for further studies to understand the relationship between different parts of the brain and any disruption in communication pathways indicative of a neural pathology.

Acknowledgment

The authors would like to thank Dr Dennis Duke of Florida State University and Dr Kerry Coburn of Mercer University for providing EEG data for this research project. The authors also would like to acknowledge Aslak Grinsted of University of Lapland, Finland, for providing part of the code used in this research.

Declaration of Conflicting Interests

The authors declared no potential conflicts of interest with respect to the research, authorship, and/or publication of this article.

Funding

The authors received no financial support for the research, authorship, and/or publication of this article.

References

- NIA. <http://www.nia.nih.gov/Alzheimers/AlzheimersInformation/GeneralInfo/>, National Institute of Aging. Accessed May 06, 2010.
- Osorio I, Frei MG. Seizure abatement with single DC pulses: Is phase resetting at play?. *Int J Neural Syst*. 2009;19(3):149–156.
- Shoeb A, Gutttag J, Pang T, Schachter S. Non-invasive computerized system for automatically initiating vagus nerve stimulation following patient-specific detection of seizures or epileptiform discharges. *Int J Neural Syst*. 2009;19(3):157–172.
- Acharya R, Chua ECP, Chua KC, Min LC, Tamura T. Analysis and automatic identification of sleep stages using higher order spectra. *Int J Neural Syst*. 2010a;20(6):509–521.
- Acharya R, Sree V, Chattopadhyay S, Yu W, Alvin APC. Application of recurrence quantification analysis for the automated identification of epileptic EEG signals. *Int J Neural Syst*. 2010b;21(3):199–211.
- Faust O, Acharya UR, Min LC, Spath BHC. Automatic identification of epileptic and background EEG signals using frequency domain parameters. *Int J Neural Syst*. 2010;20(2):159–176.
- Hsu WY. Continuous EEG signal analysis for asynchronous BCI application. *Int J Neural Syst*. 2011;21(4):335–350.
- Ihrke M, Schrobsdorff H, Herrmann JM. Recurrence-based estimation of time-distortion functions for ERP waveform reconstruction. *Int J Neural Syst*. 2010;21(1):65–78.
- Sherman D, Zhang N, Anderson M, Garg S, Hinich MJ, Thakor NV, Mirski MA. Detection of nonlinear interactions of EEG alpha waves in the brain by a new coherence measure and its application to epilepsy and anti-epileptic drug therapy. *Int J Neural Syst*. 2011;21(2):115–126.
- Ahmadlou M, Adeli H. Fuzzy synchronization likelihood for automated EEG-based diagnosis of attention-deficit/hyperactivity disorder. *Clin EEG Neurosci*. 2011;42(1):6–13.
- Jahangiri AF, Durand DM. Phase resetting of spiking epileptiform activity by electrical stimulation in the CA3 region of the rat hippocampus. *Int J Neural Syst*. 2011;21(2):127–138.
- Nelson TS, Suhr CL, Freestone DR, et al. Closed-loop seizure control with very high frequency electrical stimulation at seizure onset in the gaers model of absence epilepsy. *Int J Neural Syst*. 2011;21(2):163–173.
- Adeli H, Ghosh-Dastidar S, Dadmehr N. A spatio-temporal wavelet-chaos methodology for EEG-based diagnosis of Alzheimer's disease. *Neurosci Lett*. 2008;444(2):190–194.
- Sankari Z, Adeli H, Adeli A. Intrahemispheric, interhemispheric and distal EEG coherence in Alzheimer's disease. *Clin Neurophysiol*. 2011;122(5):897–906.
- Ahmadlou M, Adeli H, Adeli A. New diagnostic EEG markers of the Alzheimer's disease using visibility graph. *J Neural Transm*. 2010a;117(9):1099–1109.
- Ahmadlou M, Adeli H, Adeli A. Fractality and a wavelet-chaos-neural network methodology for EEG-based diagnosis of autistic spectrum disorder. *J Clin Neurophysiol*. 2010b;27(5):328–333.
- Ahmadlou A, Adeli H, Adeli A. Fractality and a wavelet-chaos methodology for EEG-based diagnosis of Alzheimer's disease. *Alzheimer Dis Assoc Disord*. 2011;25(1):85–92.
- Rizzi M, D'Aloia M, Castagnolo B. Computer aided detection of microcalcifications in digital mammograms adopting a wavelet decomposition. *Integr Comput-Aid Eng*. 2009;16(2):91–103.
- He Z, You X, Zhou L, Cheung Y, Tang YY. Writer identification using fractal dimension of wavelet subbands in gabor domain. *Integr Comput-Aid Eng*. 2010;17(2):157–165.
- Ghosh B, Basu B, O'Mahony M. Random process model for traffic flow using a wavelet - Bayesian Hierarchical technique. *Comput-Aid Civil Infrastructure Eng*. 2010;25(8):613–624.
- Boto-Giralda D, Díaz-Pernas FJ, González-Ortega D, Díez-Higuera JF, Antón-Rodríguez M, Martínez-Zarzuela M. Wavelet-based denoising for traffic volume time series forecasting with self-organizing neural networks. *Comput-Aid Civil Infrastructure Eng*. 2010;25(7):530–545.
- Lachaux JP, Lutz A, Rudrauf D, et al. Estimating the time-course of coherence between single-trial brain signals: an introduction to wavelet coherence. *Clin Neurophysiol*. 2002;32(3):157–174.
- Polikar R, Topalis A, Green D, Kounios J, Clark C. Comparative multiresolution wavelet analysis of ERP spectral bands using an ensemble of classifiers approach for early diagnosis of Alzheimer's disease. *Comput Biol Med*. 2007;37(4):542–558.

24. Adeli H, Ghosh-Dastidar S, Dadmehr N. A wavelet-chaos methodology for analysis of EEGs and EEG sub-bands to detect seizure and epilepsy. *IEEE T Biomed Eng.* 2007;54(2):205–211.
25. Torrence C, Compo GP. A practical guide to wavelet analysis. *Bull Am Meteorol Soc.* 1998;79:61–78.
26. Good LB, Sabesan S, Marsh ST, Tsakalis KS, Iasemidis LD. Control of synchronization of brain dynamics leads to control of epileptic seizures in rodents. *Int J Neural Syst.* 2009;19(3):173–196.
27. Torrence C, Webster P. Interdecadal changes in the ENSO–monsoon system. *J Climate.* 1999;12:2679–2690.
28. Grinsted A, Moore JC, Jevrejeva S. Application of the cross wavelet transform and wavelet coherence to geophysical time series. *Nonlinear Proc Geoph.* 2004;11:561–566.
29. Klein A, Sauer T, Jedynek A, Skrandies W. Conventional and wavelet coherence applied to sensory-evoked electrical brain activity. *IEEE T Biomed Eng.* 2006;53(2):266–272.
30. Sakkalis V, Oikonomou T, Pachou E, Tollis I, Micheloyannis S, Zervakis M. Time-significant wavelet coherence for the evaluation of schizophrenic brain activity using a graph theory approach. *28th Annual International Conference of the IEEE, New York 2006.* EMBS'06.
31. Adeli H, Ghosh-Dastidar S, Dadmehr N. Alzheimer's disease and models of computation: imaging, classification, and neural models. *J Alzheimer Dis.* 2005a;7(3):187–199.
32. Adeli H, Ghosh-Dastidar S, Dadmehr N. Alzheimer's disease: models of computation and analysis of EEGs. *Clin EEG Neurosci.* 2005b;36(3):131–140.
33. Pritchard WS, Duke DW, Coburn KL. Altered EEG dynamical responsivity associated with normal aging and probable Alzheimer's disease. *Dementia.* 1991;2:102–105.
34. Kramer MA, Chang FL, Cohen ME, Hudson D, Szeri AJ. Synchronization measures of the scalp EEG can discriminate healthy from Alzheimers subjects. *Int J Neural Syst.* 2007;17(2): 61–69.
35. Osterhage H, Mormann F, Wagner T, Lehnertz K. Measuring the directionality of coupling: phase versus state space dynamics and application to EEG time series. *Int J Neural Syst.* 2007;17(3): 139–148.
36. Daubechies I. Ten lectures on wavelets. *CBMS-NSF Regional Conference Series in Applied Mathematics.* Philadelphia, PA: SIAM; 1992;61.
37. Mallat S. A wavelet tour of signal processing. New York, NY: Academic; 1999.
38. Adeli H, Ghosh-Dastidar S. (in corroboration with Nahid Dadmehr) *Automated EEG-based Diagnosis of Neurological Disorders - Inventing the Future of Neurology.* Boca Raton, FL: CRC Press, Taylor & Francis; 2010.
39. Adeli H, Zhou Z, Dadmehr N. Analysis of EEG records in an epileptic patient using wavelet transform. *J Neurosci Meth.* 2003; 123(1):69–87.
40. Ghosh-Dastidar S, Adeli H. Improved spiking neural networks for EEG classification and epilepsy and seizure detection. *Integr Comput-Aid Eng.* 2007;14(3):187–212.
41. Ghosh-Dastidar S, Adeli H. Spiking neural networks. *Int J Neural Syst.* 2009a;19(4):295–308.
42. Ghosh-Dastidar S, Adeli H. A new supervised learning algorithm for multiple spiking neural networks with application in epilepsy and seizure detection. *Neural Networks.* 2009b; 22(10):1419–1431.
43. Ghosh-Dastidar S, Adeli H, Dadmehr N. Mixed-band wavelet-chaos-neural network methodology for epilepsy and epileptic seizure detection. *IEEE T Biomed Eng.* 2007;54(9):1545–1551.
44. Ghosh-Dastidar S, Adeli H, Dadmehr N. Principal component analysis-enhanced cosine radial basis function neural network for robust epilepsy and seizure detection. *IEEE T Biomed Eng.* 2008; 55(2):512–518.
45. Ahmadlou M, Adeli H. Wavelet-synchronization methodology: a new approach for EEG-based diagnosis of ADHD. *Clin EEG Neurosci.* 2010;41(1):1–10.
46. Besthorn C, Förstl H, Geiger-Kabisch C, Sattel H, Gasser T, Schreiter-Gasser U. EEG coherence in Alzheimer's disease. *Electroencephalogr Clin Neurophysiol.* 1994;90(3):242–245.
47. Locatelli T, Cursi M, Liberati D, Franceschi M, Comi G. EEG coherence in Alzheimer's disease. *Electroencephalogr Clin Neurophysiol.* 1998;106(3):229–237.
48. Bablioni C, Miniussi C, Moretti D, Vecchio F, Salinari S, Frisoni G. Cortical networks generating movement-related EEG rhythms in Alzheimer's disease: an EEG coherence study. *Behav Neurosci.* 2004;118(4):698–706.
49. Jelles B, Scheltens Ph, van der Flier WM, Jonkman WM, Lopes da Silva FH, Stam CJ. Global dynamical analysis of the EEG in Alzheimer's disease: frequency-specific changes of functional interactions. *Clin Neurophysiol.* 2008;119(4):837–841.
50. Sankari Z, Adeli H. Probabilistic neural networks for diagnosis of Alzheimer's disease using conventional and wavelet coherence. *J Neurosci Meth.* 2011;197(1):165–170.